



CHORUS

This is the accepted manuscript made available via CHORUS. The article has been published as:

## Spontaneous Electromagnetic Emission from a Strongly Localized Plasma Flow

E. M. Tejero, W. E. Amatucci, G. Ganguli, C. D. Cothran, C. Crabtree, and E. Thomas, Jr.  
Phys. Rev. Lett. **106**, 185001 — Published 6 May 2011

DOI: [10.1103/PhysRevLett.106.185001](https://doi.org/10.1103/PhysRevLett.106.185001)

# Spontaneous electromagnetic emission from a strongly localized plasma flow

E. M. Tejero,<sup>1,3</sup> W. E. Amatucci,<sup>2</sup> G. Ganguli,<sup>2</sup> C. D. Cothran,<sup>1</sup> C. Crabtree,<sup>2</sup> and E. Thomas, Jr.<sup>3</sup>

<sup>1</sup>Global Strategies Group, Crofton, MD 21114

<sup>2</sup>Plasma Physics Division, Naval Research Laboratory, Washington, DC 20375

<sup>3</sup>Physics Department, Auburn University, Auburn, AL 36849

Laboratory observations of electromagnetic ion cyclotron waves generated by a localized transverse dc electric field are reported. Experiments indicate that these waves result from a strong  $\mathbf{E} \times \mathbf{B}$  flow inhomogeneity in a mildly collisional plasma with sub-critical magnetic field-aligned current. The wave amplitude scales with the magnitude of the applied radial dc electric field. The electromagnetic signatures become stronger with increasing plasma  $\beta$ , and the radial extent of the power is larger than that of the electrostatic counterpart. Near-Earth space weather implications of the results are discussed.

We report laboratory observations of spontaneously generated electromagnetic ion cyclotron (EMIC) waves associated with highly sheared plasma flows transverse to the background magnetic field. Theory [1, 2] and previous laboratory experiments [3–8] have shown that sufficiently strong sheared flows can drive electrostatic ion cyclotron waves by generating strong inhomogeneity in the energy density. The electrostatic waves have been shown to be broadband, Doppler-shifted near the ion cyclotron frequency, primarily propagating transverse to the magnetic field, and spatially localized to the velocity shear layer. Transverse ion heating of factors of 2-4 have been observed as a result of these waves [9, 10]. Such transverse ion heating is an important first step in the formation of ion conics and the bulk transport of ions, which can impact near-Earth space weather [11].

A variety of space observations have revealed that inhomogeneities, such as small scale, transverse electric field structures [12, 13] and sheared flows [14–16], are important in space plasmas [17–20]. Alfvén waves propagating into the ionosphere from the magnetosphere can form quasistatic electric fields transverse to the magnetic field by wave steepening processes [21–23]. The electrostatic instabilities produced by these electric fields are thought to dissipate their power in the ionosphere and produce localized ion heating. Electromagnetic instabilities due to such localized transverse electric field structures have also been predicted [24], but they have not been experimentally investigated. Such locally generated EMIC waves could affect broader ionospheric and magnetospheric dynamics by heating remote ions and convecting energy far from the region of wave creation. Our objective was to design a laboratory experiment to study the generation and character of electromagnetic fluctuations due to inhomogeneity in transverse plasma flows.

This Letter presents experimental results that identify EMIC waves that are driven by strongly sheared flows. The EMIC wave amplitude increases with increasing plasma  $\beta$  and the Doppler-shifted frequency is resonant with a harmonic of the ion-cyclotron frequency. Wave vector measurements indicate predominantly  $m = 1$  azimuthal mode propagation, similar to simultaneously

cited shear-driven electrostatic ion cyclotron waves, but with longer wavelength. The EMIC waves exhibit the same frequency content as the electrostatic waves, and the wave peak amplitude is co-located with a peak in the velocity shear. Finally, in contrast to the electrostatic waves that were also measured, the EMIC waves are observed to extend far from the source region across the magnetic field.

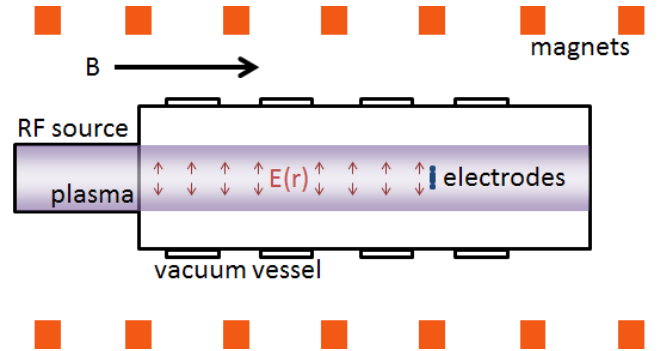


FIG. 1. Schematic of the experiment showing the location of the electrodes.

The experiments were conducted in the source chamber section of the Space Physics Simulation Chamber (SPSC) at the Naval Research Laboratory, which is shown in Figure 1. The source chamber is a 2-m long, 55-cm diameter cylindrical vacuum chamber with an inductively coupled RF plasma source, typically operated at 14.2 MHz and up to 600 W. The operational parameters for the steady-state argon plasma are plasma density  $n \approx 10^9 - 10^{11} \text{ cm}^{-3}$ , ion and electron temperatures  $T_i \approx 0.05 \text{ eV}$  and  $T_e \approx 3 - 5 \text{ eV}$ , uniform axial magnetic field  $B = 300 \text{ G}$ , ion cyclotron frequency  $f_{ci} = 11.5 \text{ kHz}$ , ion gyroradius  $\rho_i = 0.3 \text{ cm}$ , ion thermal speed  $v_{ti} \approx 5 \times 10^4 \text{ cm/s}$ , and Debye length  $\lambda_D \approx 0.01 \text{ cm}$ . The ion-neutral collision frequency is  $\nu_{in} \approx 3.9 \times 10^3 \text{ s}^{-1}$  for a neutral density of  $n_n \approx 1 \times 10^{13} \text{ cm}^{-3}$ . The electron plasma frequency to electron cyclotron frequency ratio for the SPSC scales favorably to the auroral ionosphere ( $\omega_{pe}/\Omega_{ce})_{ionosphere} \approx 0.1 - 10$  and ( $\omega_{pe}/\Omega_{ce})_{SPSC} \approx$

0.2 – 3.4. The effective plasma column diameter and length are 16 cm and 125 cm, respectively. Wave and bulk plasma parameters are measured using Langmuir probes, double probes, three-axis  $\hat{\mathbf{B}}$  loops, and emissive probes. The  $\hat{\mathbf{B}}$  loops are electrostatically shielded so that only the electromagnetic waves contribute to the inductive electric fields that they measure. Electrostatic fluctuations are detected as oscillations in the ion saturation current on Langmuir probe tips.

The double,  $\hat{\mathbf{B}}$ , and emissive probes are attached to independent radial translation stages mounted to three orthogonal vacuum ports that are axially located on a plane 20 cm in front of the biasable electrodes used to generate the radial electric field. The electrodes consist of a 2-cm diameter center disk and an isolated 0.6-cm wide annulus with an outer diameter of 3.8 cm. The radial gap between the electrodes is 0.3 cm. For the set of experiments described in this Letter the annulus was biased while the center disk was not connected resulting in an inhomogeneous radial electric field that switches from radially inward to radially outward across the outer electrode. This arrangement produces strongly sheared azimuthal flows.

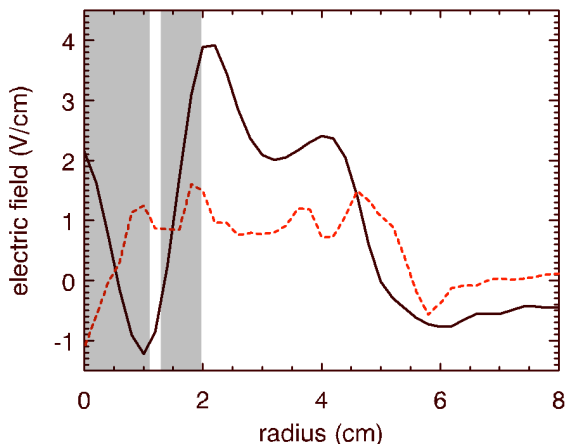


FIG. 2. This figure shows typical cylindrically symmetric, radial electric field profiles: background profile (dashed line) with the electrodes disconnected and the profile with the annulus biased to 150 V (solid line) leaving the center disk disconnected. The shaded regions indicate the position of the electrodes.

Plasma potential was measured using the floating potential of an emissive probe heated to a highly emissive state. Electric field profiles were determined by numerically differentiating the plasma potential profiles and can be seen in Figure 2. The cylindrically symmetric electric field has a maximum value  $E_{peak} \approx 4$  V/cm and a scale size  $L_E \equiv \left(\frac{1}{E} \frac{dE}{dr}\right)^{-1} \approx 1.7\rho_i$ . The observed ratio of ion gyroradius to electric field scale length is close to the upper range of that observed in the space

( $\rho_i/L_E$ )<sub>ionosphere</sub>  $\approx 0.01 - 0.5$  [20] and ( $\rho_i/L_e$ )<sub>SPSC</sub>  $\approx 0.6$ . The combination of this radial electric field and the background axial magnetic field causes a cylindrically symmetric azimuthal plasma flow due to the  $\mathbf{E} \times \mathbf{B}$  drift. The inhomogeneity in the radial electric field results in radial shear in the azimuthal velocity profile, which extends along the length of the device and is the source of the free energy to drive the observed instabilities. The normalized shear frequency  $\frac{\omega_s}{\Omega_{ci}} \equiv \frac{1}{\Omega_{ci}} \frac{dv_E}{dr}$  characterizes the shear in the flow, where  $v_E$  is the  $\mathbf{E} \times \mathbf{B}$  drift. In the ionosphere, estimated values for the normalized shear frequency up to 6 have been observed [11] and values greater than 10 can be created in the laboratory.

Under plasma conditions with low  $\beta$  ( $\equiv \frac{nkT}{B^2/2\mu_0}$ ) and sufficiently strong, localized electric fields, velocity shear-driven electrostatic ion cyclotron waves are observed to have characteristics consistent with previous experimental results [11]. By increasing the plasma  $\beta$  while maintaining sufficiently strong sheared flows, electromagnetic waves near the ion cyclotron frequency have been observed using 3-axis  $\hat{\mathbf{B}}$  loops. The electrostatic and electromagnetic oscillations have similar spectral signatures. The inset of Figure 3 shows a typical power spectrum for the observed electromagnetic mode with frequency below the ion cyclotron frequency  $f/f_{ci} \approx 0.65 - 0.85$ , broadband character  $\Delta f/f \approx 0.1 - 0.15$ , and the “spiky” spectral structure characteristic of the inhomogeneous energy-density driven instability (IEDDI) [3–6, 25, 26]. The amplitudes of the wave magnetic field components are roughly equal, with the total magnetic field fluctuation amplitude  $B_1 \approx 0.25 \mu\text{T}$ . The wave electric field was approximated using the measured electrostatic wave potential as  $E_1 = k\phi_1 \approx 2$  V/m. This resulted in an  $E_1/B_1$  ratio of approximately ten times the Alfvén speed. Figure 3 shows a comparison of radial profiles of normalized wave amplitude for the electrostatic (dashed line) and electromagnetic fluctuations (solid line). The outer electrode was biased to 150 V relative to chamber ground, while the center disk was disconnected. Both profiles indicate a spatial localization to regions of strong velocity shear, where the inhomogeneous electric field was present. However, the electromagnetic profile shows significant wave power outside the shear layer.

A series of scans were performed, changing the plasma  $\beta$  by scanning RF power and the magnetic field. The current oscillations remained constant for a wide range of  $\beta$  throughout these scans. A minimum  $\beta$  level for noticeable EMIC wave amplitude was found that remained constant within experimental error for a wide range of density and magnetic field strengths, resulting in a range of  $\beta$  from  $1.0 \times 10^{-6}$  to  $5 \times 10^{-5}$ . The electromagnetic wave amplitude increased by an order of magnitude above the noise floor over this range in  $\beta$ .

The wave vector components for the electromagnetic waves were determined using the Fourier transform of

the cross-correlation function to measure the phase difference between the time series of the same magnetic field component of two spatially separated  $\vec{B}$  probes [27]. The measurement of the radial wave number indicated outward radial propagation with  $k_r = 0.168 \pm 0.008 \text{ cm}^{-1}$ . The axial wave number measurement, made at three unequally spaced axial points, at the center of the chamber indicated a propagation direction parallel to  $B$  with  $k_z = 0.05 \pm 0.007 \text{ cm}^{-1}$ . Measurements of azimuthal mode number outside the shear layer are consistent with an  $m = 1$  cylindrical mode, rotating in the direction of the azimuthal flow.

Peñano and Ganguli [28] developed a model that describes small-amplitude electromagnetic ion cyclotron waves in the presence of a localized inhomogeneous transverse electric field and a uniform background magnetic field. They numerically solved the resulting system of eigenvalue equations in order to analyze the stability and physical properties of velocity shear-driven electromagnetic ion cyclotron waves. For long parallel wavelength, the instability is an electromagnetic Kelvin-Helmholtz mode, and the peak amplitude of the eigenfunction is localized about the center of the flow layer where  $\partial v_E / \partial r = 0$  and  $\partial^2 v_E / \partial r^2$  is maximum. For short parallel wavelength, the instability is an ion cyclotron mode, and the peak amplitude of the eigenfunction is localized to the region where  $\partial v_E / \partial r < 0$ . In Figure 4, the top panel shows the normalized magnetic (solid) and electrostatic (dashed) fluctuation amplitudes as a function of radius. The bottom panel shows the normalized shear frequency (solid) and the normalized density gradient (dashed),

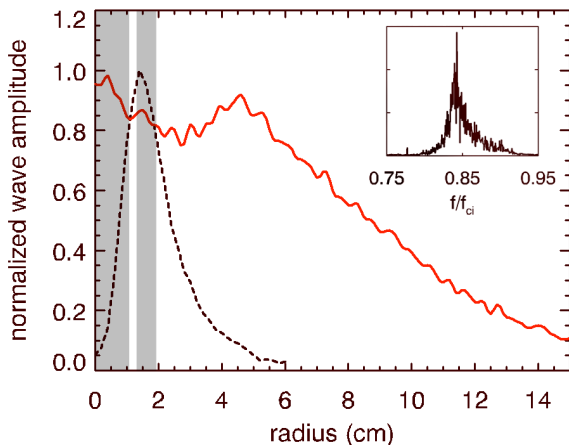


FIG. 3. Profiles of normalized wave amplitude as a function of radial position are shown, where the dashed line and the solid line depict the electrostatic ( $\delta n / \delta n_{max}$ ) and electromagnetic ( $\delta B / \delta B_{max}$ ) fluctuations respectively. The shaded regions indicate the positions of the electrodes. The inset is a typical power spectrum of the magnetic fluctuations.

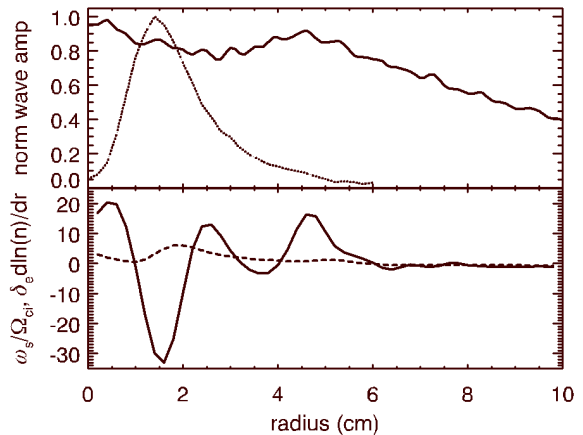


FIG. 4. The solid and dashed lines in the top plot are the radial profiles of the normalized magnetic and electrostatic fluctuation amplitude respectively. The bottom plot shows radial profiles of shear frequency (solid) and normalized density gradient (dashed).

$\delta_e \frac{\partial \ln(n)}{\partial r}$  as a function of radius, where  $\delta_e = c / \omega_{ce}$  is the electron skin depth. The peak mode amplitudes are spatially co-located with regions of large velocity shear suggesting that the modes are velocity shear-driven ion cyclotron waves. There is a region containing a density gradient near the peak mode amplitude of the electrostatic mode, but it is much milder than the electric field gradient.

Figure 5 shows the behavior of the normalized mode amplitude (solid line) as a function of the bias applied to the outer electrode, indicating a threshold for the wave. A comparison of the fractional change in the electric field (circles) and the density gradient (triangles) as functions of bias demonstrates a clear correlation between the growth of the mode and the electric field. The reference values at threshold are  $E_0 = 60.5 \text{ V/m}$  and  $(\partial \ln n / \partial r)_0 = 19.5 \text{ m}^{-1}$ . The electric field has a factor of four change over a small bias range just above threshold, while the density gradient is relatively constant. This supports the identification of the mode as being shear-driven and not a drift wave.

In order to further test whether the electromagnetic wave and the electrostatic wave are created by the same shear-driven instability, a bias scan of the outer electrode was conducted. Changing the bias on the electrodes changed the radial electric field and thus the flow shear, which resulted in a different frequency for the observed mode. The inset in Figure 5 shows that the frequency of the electromagnetic wave tracks the frequency of the electrostatic wave.

The parallel electron drift velocity was estimated from measurements of the field-aligned current (FAC) col-

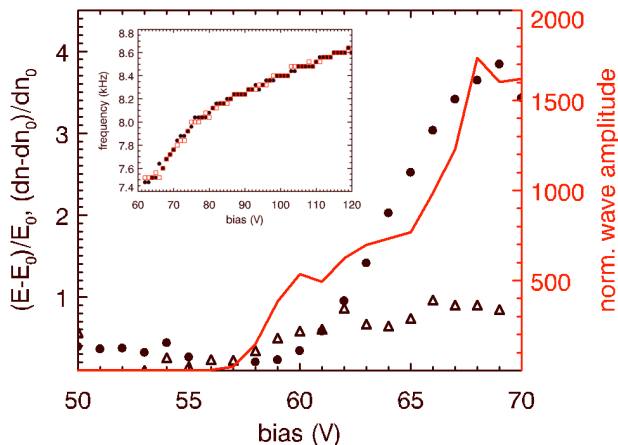


FIG. 5. Normalized wave amplitude (solid line), fractional electric field (filled circles),  $(E - E_0)/E_0$ , and fractional density gradient (open triangles),  $(\partial \ln n / \partial r - (\partial \ln n / \partial r)_0) / (\partial \ln n / \partial r)_0$ , as a function of applied ring bias. The inset is a plot of observed frequency as a function of the bias: peak frequency of electrostatic fluctuations (filled circles) within the shear layer and magnetic fluctuations (open squares) at the edge of the plasma column.

lected by the electrodes,  $v_d \approx 16$  km/s. This was compared to the critical drift velocity for the current-driven ion cyclotron instability in the presence of collisions. The weakly collisional limit of the theory by *Satyanarayana et al.* [29] predicts a critical drift velocity  $v_c \approx 550$  km/s for our experimental parameters, which is more than 30 times larger than the estimated electron drift in the experiment. The observed mode can not be current driven.

Our experiment establishes that strongly localized dc electric fields perpendicular to the ambient magnetic field can behave as a radiation source for EMIC waves, which can transport the energy away from the region of wave generation. The results are consistent with the theory of Peñano and Ganguli [28].

Alfvén waves carry energy and momentum from the distant magnetosphere to the near-Earth region, where they can steepen to form localized electric fields. It is generally assumed that the Earth-directed energy and momentum flux is ultimately dissipated in the near-Earth region in the form of Joule heating, which affects the near-Earth plasma state and hence space weather. Our experiment suggests that not all the energy and momentum that reaches the ionosphere may be dissipated as local heating. A fraction of the energy may be radiated back into the magnetosphere. Satellites have observed anti-Earthward Poynting flux [30], indicating the existence of a radiation source beneath the satellite altitude.

This work was supported by the Office of Naval Research, NASA, and the Defense Threat Reduction Agency.

- 
- [1] G. Ganguli, Y. C. Lee, and P. Palmadesso, *Phys. Fluids* **28**, 761 (1985).
  - [2] G. Ganguli, Y. C. Lee, and P. J. Palmadesso, *Phys. Fluids* **31**, 823 (1988).
  - [3] M. E. Koepke, W. E. Amatucci, J. J. Carroll III, and T. E. Sheridan, *Phys. Rev. Lett.* **72**, 3355 (1994).
  - [4] W. E. Amatucci, M. E. Koepke, J. J. Carroll III, and T. E. Sheridan, *Geophys. Res. Lett.* **21**, 1595 (1994).
  - [5] M. E. Koepke, W. E. Amatucci, J. J. Carroll III, V. Gavrishchaka, and G. Ganguli, *Phys. Plasmas* **2**, 2523 (1995).
  - [6] W. E. Amatucci *et al.*, *Phys. Rev. Lett.* **77**, 1978 (1996).
  - [7] E. Thomas, Jr., J. D. Jackson, E. A. Wallace, and G. Ganguli, *Phys. Plasmas* **10**, 1191 (2003).
  - [8] S. Kim, E. Agrimson, M. J. Miller, N. D'Angelo, and R. L. Merlino, *Phys. Plasmas* **11**, 4501 (2004).
  - [9] D. N. Walker, W. E. Amatucci, G. Ganguli, J. A. Antoniadis, J. H. Bowles, and D. Duncan, *Geophys. Res. Lett.* **24**, 1187 (1997).
  - [10] W. E. Amatucci *et al.*, *J. Geophys. Res.* **103**, 11711 (1998).
  - [11] W. E. Amatucci, *J. Geophys. Res.* **104**, 14481 (1999).
  - [12] F. S. Mozer *et al.*, *Phys. Rev. Lett.* **38**, 292 (1977).
  - [13] F. S. Mozer, R. Ergun, M. Temerin, C. Cattell, J. Dombek, and J. Wygant, *Phys. Rev. Lett.* **79**, 1281 (1997).
  - [14] J. Providakes, D. Farley, W. Swartz, and D. Riggan, *J. Geophys. Res.* **90**, 7513 (1985).
  - [15] B. G. Fejer and J. F. Providakes, *Phys. Scr.* **T18**, 167 (1987).
  - [16] H. Liu and G. Lu, *Ann. Geophysicae* **22**, 1149 (2004).
  - [17] J. E. Maggs and T. N. Davis, *Planet. Space Sci.* **16**, 205 (1968).
  - [18] M. C. Kelley and C. W. Carlson, *J. Geophys. Res.* **82**, 2343 (1977).
  - [19] M. Temerin *et al.*, *J. Geophys. Res.* **86**, 11278 (1981).
  - [20] M. Hamrin *et al.*, *J. Geophys. Res.* **106**, 10803 (2001).
  - [21] E. V. Mishin and M. Förster, *Geophys. Res. Lett.* **22**, 1745 (1995).
  - [22] R. Lysak and Y. Song, *J. Geophys. Res.* **101**, 15411 (1996).
  - [23] C. E. Seyler, A. E. Clark, J. Bonnell, and J.-E. Wahlund, *J. Geophys. Res.* **103**, 7027 (1998).
  - [24] J. R. Peñano and G. Ganguli, *Phys. Rev. Lett.* **83**, 1343 (1999).
  - [25] V. Gavrishchaka, M. E. Koepke, and G. Ganguli, *Phys. Plasmas* **3**, 3091 (1996).
  - [26] K.-I. Nishikawa, G. Ganguli, Y. C. Lee, and P. J. Palmadesso, *Phys. Fluids* **31**, 1568 (1988).
  - [27] D. E. Smith, E. J. Powers, and G. S. Caldwell, *IEEE Trans. Plasma Sci.* **2**, 261 (1974).
  - [28] J. R. Peñano and G. Ganguli, *J. Geophys. Res.* **107**, 1189 (2002).
  - [29] P. Satyanarayana, P. K. Chaturvedi, M. J. Keskinen, J. D. Huba, and S. L. Ossakow, *J. Geophys. Res.* **90**, 12209 (1985).
  - [30] N. Ivchenko *et al.*, *Geophys. Res. Lett.* **26**, 3365 (1999).